Report
P-20-18
August 2020

EBS TF – THM modelling

Water transport in pellets-filled slots – evaluation of model contributions

Mattias Åkesson

SVENSK KÄRNBRÄNSLEHANTERING AB

SWEDISH NUCLEAR FUEL
AND WASTE MANAGEMENT CO

Box 3091, SE-169 03 Solna
Phone +46 8 459 84 00
skb.se

SVENSK KÄRNBRÄNSLEHANTERING

ISSN 1651-4416
SKB P-20-18
ID 1900483

August 2020

EBS TF – THM modelling

Water transport in pellets-filled slots – evaluation of model contributions

Mattias Åkesson, Svensk Kärnbränslehantering AB

Abstract

This report presents an evaluation of all contributions that has been performed for the modelling task "Water transport in pellets-filled slots" within the EBS Taskforce. The aim of this task was to investigate the ability of models (existing or new) to simulate water transport at different test conditions. Two subtasks have addressed two test types: A) 1D-tests with water freely available (water uptake tests), and C) 1D-tests with water redistribution in a temperature gradient. Tests were performed with two different pellets materials: extruded Asha NW BFL-L and roller compacted MX-80.

The following modelling teams have contributed to the task and have been using different numerical codes: i) the SKB team, using COMSOL Multiphysics; ii) the RWM team, from Wood Nuclear Limited, using COMSOL Multiphysics and TOUGH2; iii) the SKB1 team, from Clay Technology AB, using Code_Bright; and iv) the POSIVA team from UCLM, using COMSOL Multiphysics as implementation platform. The used material models included established constitutive relations: i) water retention curves; ii) the Darcy´s law for unsaturated liquid transport; and iii) vapour diffusion. Results show that the processes in Test A and C can be described with these relations.

Sammanfattning

Denna rapport presenterar en utvärdering av samtliga bidrag som har utförts till modelleringsuppgiften Task 10 ”Vattentransport i pelletsfyllda spalter” inom samarbetsprojektet ”Task Force on Engineered Barrier Systems”. Målet med denna uppgift var att undersöka olika (befintliga eller nya) materialmodellers förmåga att simulera vattentransport under olika testförhållanden. Två deluppgifter har inriktats mot två testtyper: A) 1D-tester med fri tillgång på vatten (vattenupptagsförsök), och C) 1D-tester med fuktomfördelning i en temperaturgradient. Testerna utfördes med två olika pelletsmaterial: extruderad Asha NW BFL-L, och rullkompakterad MX-80.

Följande modelleringsgrupper har bidragit till uppgiften och har använt olika numeriska koder: i) SKB-teamet med COMSOL Multiphysics; ii) RWM-teamet, från Wood Nuclear Limited, med COMSOL Multiphysics och TOUGH2; iii) SKB1-teamet, från Clay Technology AB med Code_Bright; och iv) POSIVA-teamet, från UCLM med COMSOL Multiphysics som implementationsplattform. De använda materialmodellerna innefattade etablerade konstitutiva samband: i) vattenretentionskurvor; ii) Darcy´s lag för omättad vätsketransport; samt iii) ångdiffusion. Resultaten visar att processerna i Test A och C kan beskrivas med dessa samband.

Contents

1 Introduction

A modelling task denoted “Water transport in pellets-filled slots” was defined within the framework of EBS Taskforce during 2016. The aim of this was to formulate new models or use existing models for water transport in pellet fillings and to calibrate and check their ability to model water transport at different boundary and inflow conditions and at different temperature situations.

Four different subtasks were originally proposed:

- Subtask A. 1D-tests with water freely available (water uptake tests).
- Subtask B. Constant water inflow rate from point inflow.
- Subtask C. 1D-tests with water redistribution in a temperature gradient.
- Subtask D. 1D-tests with water freely available in a temperature gradient.

These subtasks were planned to be based on experimental data from four corresponding test types. However, due to limited resources, only tests within two of the subtasks (A and C) could be performed and included in the task description, which was distributed in September 2016. This description was subsequently complemented with results for two additional Subtask C tests, which were finalized and distributed in March 2019. A task description for subtask B was distributed in June 2018. This was based on experimental work financed by Posiva Oy which will be published elsewhere.

This report presents an evaluation of the contributing modelling work that has been performed within the framework of this task. The following modelling teams, using different numerical codes, have contributed and submitted results:

- SKB team, using COMSOL Multiphysics.
- RWM team, using COMSOL Multiphysics and TOUGH2.
- SKB1 team, using Code_Bright.
- POSIVA team, using COMSOL Multiphysics.

A description of subtasks A and C, and the requested results are presented in Chapter 2. A compilation of contributions, material models and modelling approaches is presented in Chapter 3. A compilation and a discussion of modelling results are presented in Chapter 4. Finally, concluding remarks regarding the capabilities and deficiencies of the material models concerning water transport in pellets are given in Chapter 5.

2 Task descriptions

This chapter presents a short overview of the laboratory tests, the test results, the used pellets materials and the requested model results. A more detailed description of these tests is given by Åkesson et al. (2020).

2.1 Bentonite pellets

Two types of pellets were used in the tests:

- **Extruded 6 mm rods (Asha NW BFL-L).** This bentonite is produced by Ashapura Minechem Co and is quarried in the Kutch area on the northwest coast of India. The raw material was delivered to SKB in 2010 and 2012. The pellets were manufactured at Äspö HRL by extrusion (i.e. pressed through a hole-matrix), which results in pellets shaped as rods with varying length.
- **Compacted pillows (MX-80-11).** MX-80 is a Wyoming-type bentonite supplied by the American Colloid Company. The pellets were manufactured by HOSOKAWA Bepex GmbH in Germany, using a roller compaction technique where the material is compacted between two counter-rotating wheels with cut-outs, which results in compacted pillow-shaped pellets.

Both bentonites are sodium dominated, and both pellet types were sieved in order to remove all fines.

The particle density of the Asha bentonite was 2 920 kg/m^3. The corresponding value for the MX-80 bentonite was 2 780 kg/m^3.

The initial bulk dry density and water content may have varied slightly between the different tests. In general, the Asha pellets had a dry density of 958 kg/m^3 and a water content of 14.7 %. The corresponding value for the MX-80 bentonite was 953 kg/m^3 and 14.5 %, respectively.

2.2 Subtask A

The subtask A tests have yielded information about the water transport when the pellet filling controls the inflow rate. Plexiglas cylinders, 50 cm long and with the inner diameter 10 cm were used for the tests. Tap water was available in a filter in the bottom. The top of the cylinder was sealed with a lid, which in turn was connected to a flexible balloon with the purpose of avoiding a gas pressure build-up.

Figure 2-1 shows a schematic drawing of the test arrangements. The tests were run for different times and the water content profile was measured at the end of each test. The two types of pellets described above were used in the tests.

The filter in the bottom of the tube was connected to a reservoir with a water surface fixed at a defined level above the filter. The reason for this was to ensure that proper contact was reached between the water and the pellets filling. The constant head was upheld with a peristaltic pump which continuously supplied water from an external reservoir. A head of 1–2 cm (corresponding to 0.1–0.2 kPa) was used in the short-term tests, whereas a head of 10 cm (1 kPa) was used in the long-time tests Ar3 and Ae3 (“e” denotes extruded pellets, i.e. Asha, and “r” denotes roller compacted, i.e MX-80).

Measurement of the relative humidity (RH) were made in three points, located 3, 8 and 15.5 cm above the filter, in one of the tests (Ar3). The water uptake (q) was measured by weighing the external reservoir for each test regularly.

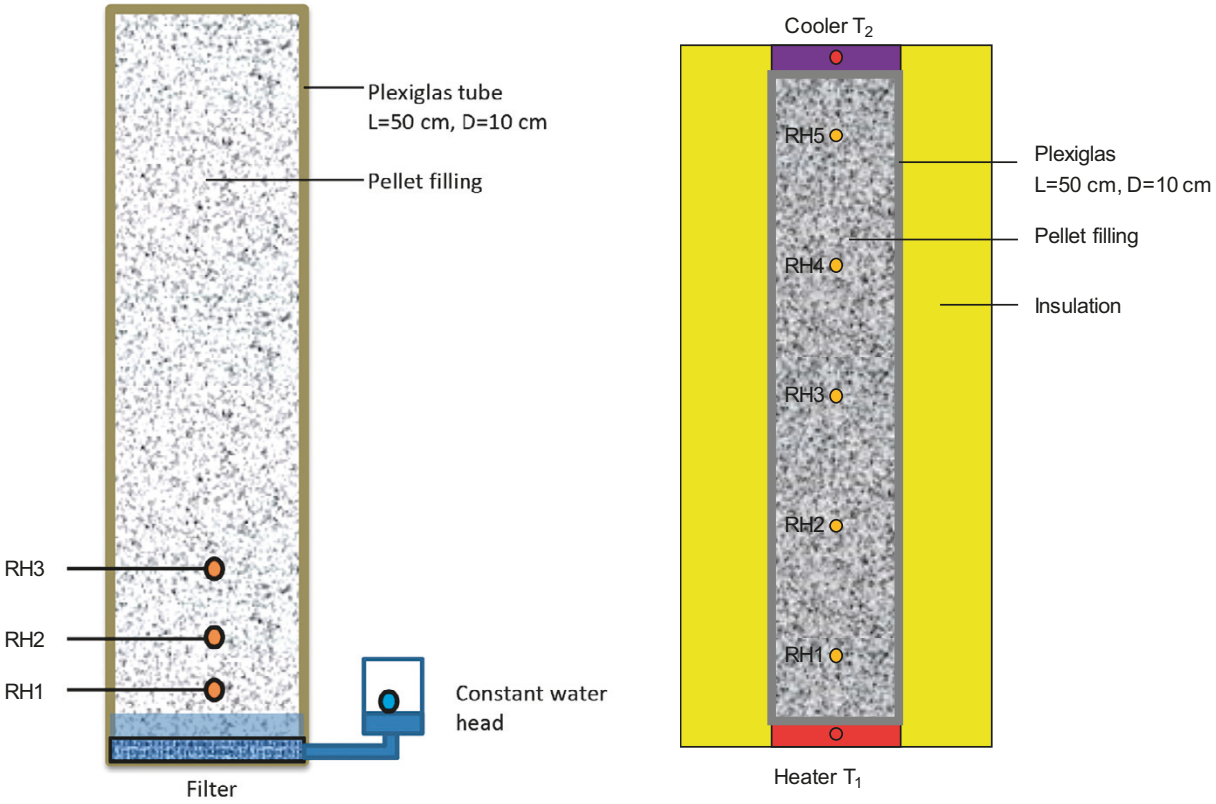

Figure 2-1. *Test arrangement for test type A (left) and type C (right).*

Water content profiles for the regular tests (Ar1-3 and Ae1-3) are shown in Figure 2-2 and Figure 2-3. The evolution of the cumulative water uptake in the regular long-term tests (Ar3 and Ae3) is shown in Figure 2-4. The evolution of RH in the Ar3 test is shown in Figure 2-5.

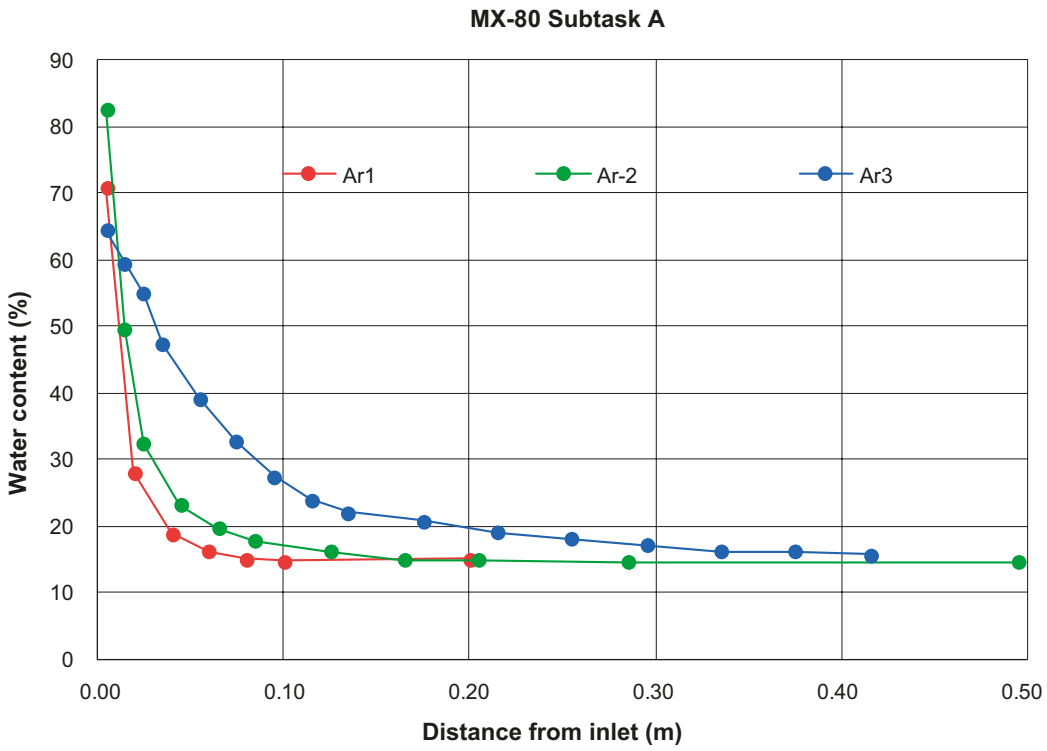

Figure 2-2. *Water content profiles at the end of test Ar1-Ar3.*

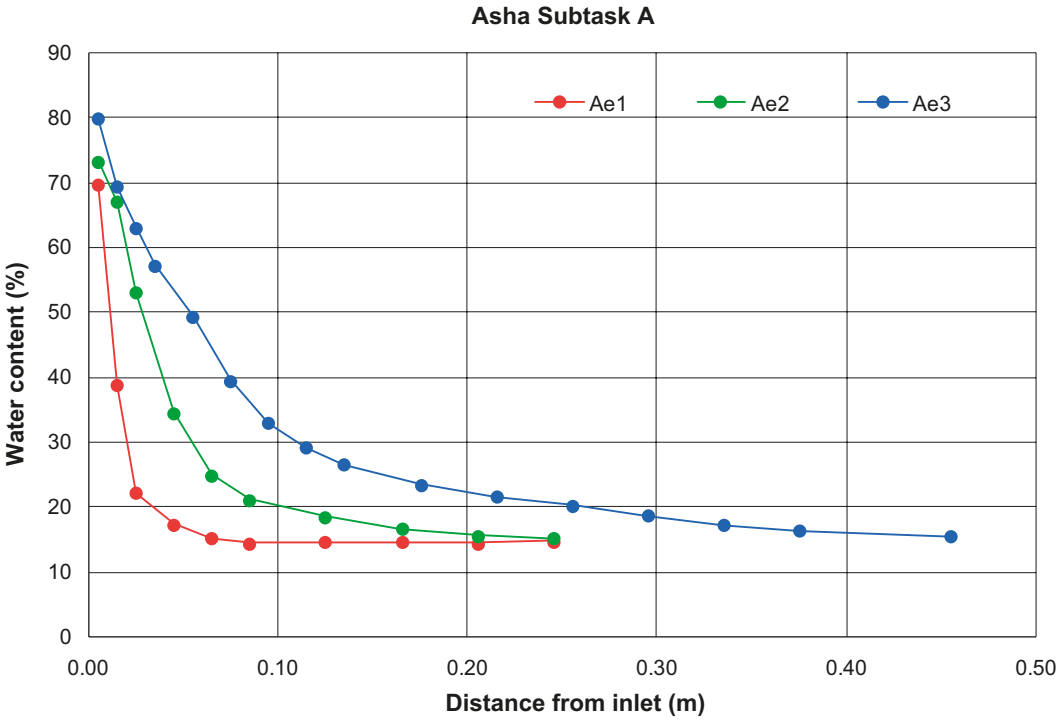

Figure 2-3. *Water content profiles at the end of test Ae1-Ae3.*

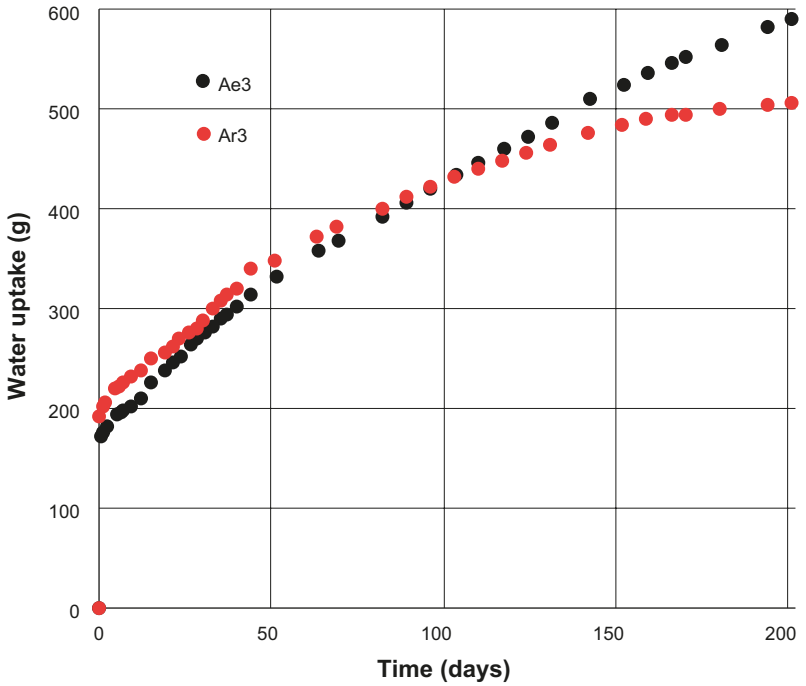

Figure 2-4. *Measured water uptake versus time.*

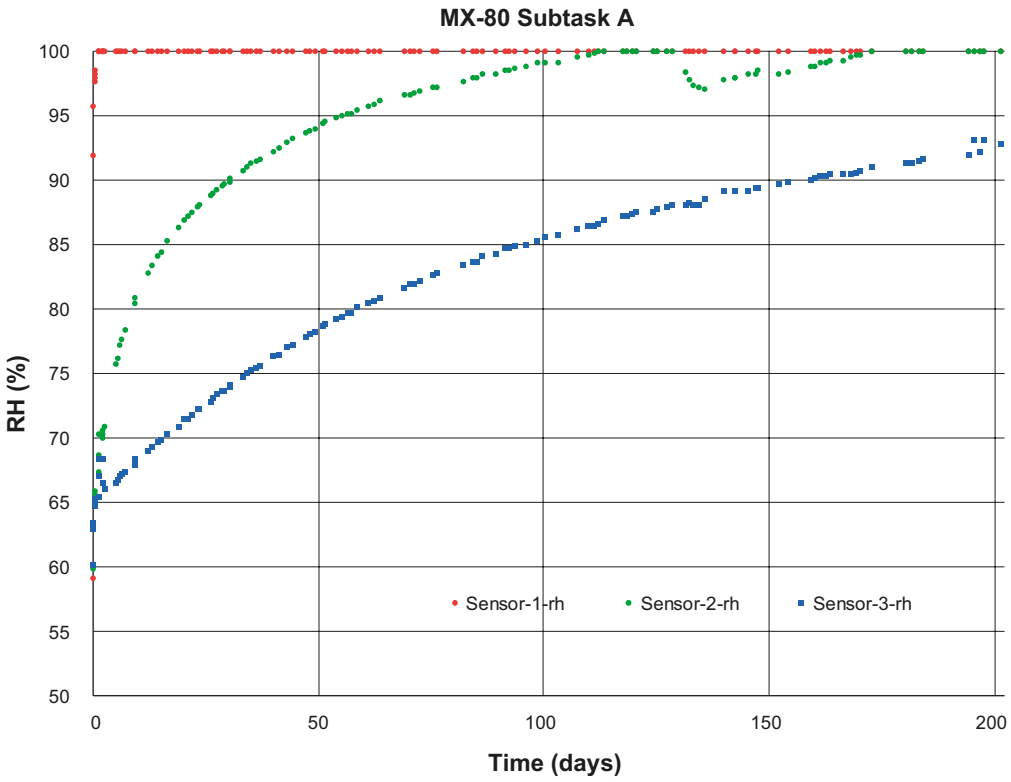

Figure 2-5. *Measured RH versus time in test Ar3. Sensors 1, 2 and 3 were located 3, 8 and 15.5 cm from water inlet, respectively.*

It should be noted that the initial discrete increase of the cumulative water uptake observed in the long-term tests (Figure 2-4) corresponded to the applied water pressure at the inlet. This means that the large pores between pellets within approximately 5 cm from the inlet were flooded at the start. This is also reflected by the rapid RH increase at the sensor located 3 cm from the inlet in Ar3. It should also be noted that the final measured cumulative water uptake values were found to be significantly higher than corresponding values based on the final water content profiles, which were found to be 317 and 436 grams for Ar3 and Ae3, respectively (see Åkesson et al. 2020). The most likely cause of this was that the measured data was influenced by different types of evaporation and leakage.

Table 2-1. Final test matrix for test type A.

Test	Pellet type	Duration	Meas.	Water pressure
Ar1	RC MX-80	5 days (120 h)	q	0.1 kPa
Ar2	RC MX-80	30 days (720 h)	q	0.2 kPa
Ar3	RC MX-80	203 days (4 872 h)	RH, q	1.0 kPa
Ae1	Ex Asha	5 days	q	0.2 kPa
Ae2	Ex Asha	30 days	q	0.2 kPa
Ae3	Ex Asha	202 days (4 848 h)	q	1.0 kPa

2.3 Subtask C

The subtask C tests have given basic information about how moisture is redistributed in a temperature gradient. The tests were performed in a 50 cm long Plexiglass cylinder with a diameter of 10 cm, similar to the ones in the type A tests. No free water was however available. Instead, a temperature gradient was applied along the axis of the cylinder, which were thermally insulated, heated at the bottom and cooled at the top. Measurements of RH and temperature were made in all tests (RH and temperature in 5 and 7 points, respectively). Figure 2-1 shows a schematic drawing of the test arrangements. The same test equipment was used for all tests.

The tests were run for different times. Table 2-2 shows the actual test matrix carried through.

The temperature on the heater side and the cooled side was in all test 74 and 24 °C, respectively. For the long-term tests which were run for 90 days or more, the lateral surface of the cylinder was thermally insulated with approx. 14 cm of mineral or glass wool inside a plastic cylinder with a 39 cm inner diameter.

The tube was instrumented with five RH sensors (Aitemin SHT75 V3) which were placed at the distance 5, 15, 25, 35 and 45 cm from the heated bottom plate. Temperature was measured by the RH sensors, on (or inside) the bottom plate, and on the cooling flanges on the top plates. The bottom plate was heated with a temperature controlled hot plate. The cooling was achieved by flanges attached to the top plate in contact with the room atmosphere.

The water content distribution was determined after the termination of each test.

The dry density of the pellets filling in the two additional tests was 958 kg/m^3 (Cr3d) and 992 kg/m^3 (Cr3e).

Evolutions of sensors data from test Ce3d regarding temperature and RH are shown in Figure 2-6 and Figure 2-7, respectively, and the water content profile measured at the end of this test is shown in Figure 2-8. Corresponding results for tests Cr3d and Cr3e are shown in Figure 2-9 to Figure 2-11.

Table 2-2. Final test matrix for test type C.

Test	Pellet type	T_1/T_2	Test duration	Meas.	Remarks
Cr1	RC MX-80	74/24	5 h	T, RH	Uncertain
Cr3b	RC MX-80	74/24	7 days (169 h)	T, RH	
Cr3c	RC MX-80	74/24	14 days (331 h)	T, RH	Uncertain
Cr3d	RC MX-80	74/24	91 days	T, RH	
Cr3e	RC MX-80	74/24	364 days	T, RH	
Ce3d	Ex Asha	74/24	90 days (2161 h)	T, RH	

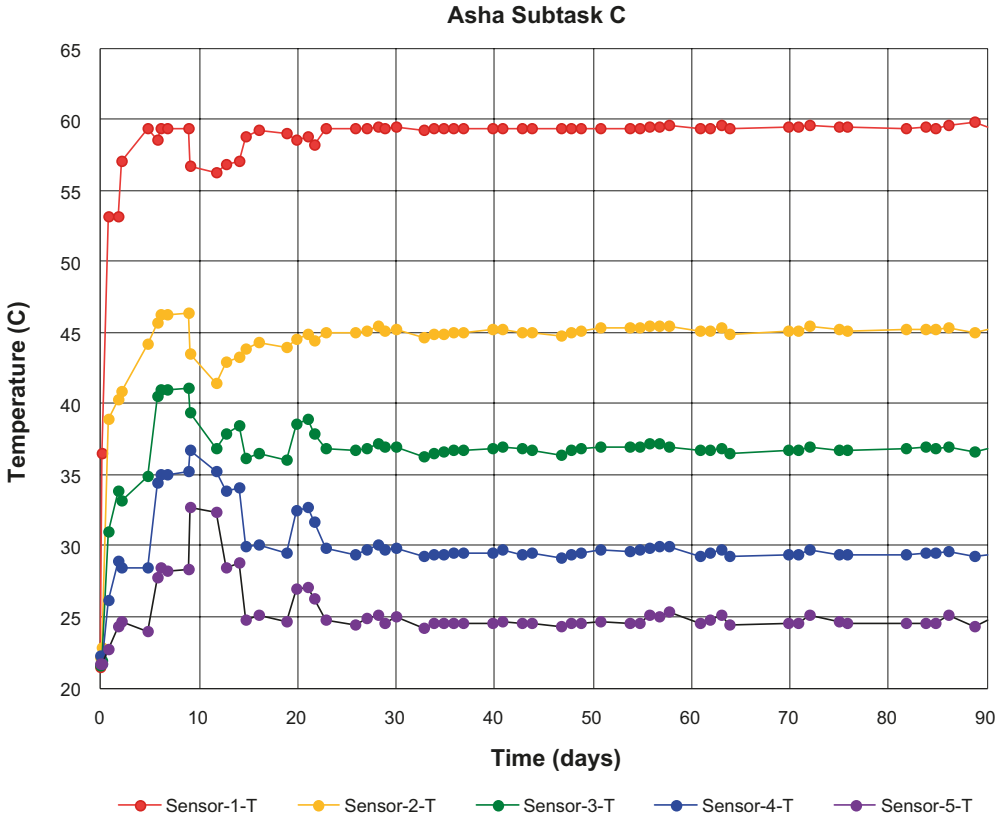

Figure 2-6. *Measured temperature vs time in test Ce3d.*

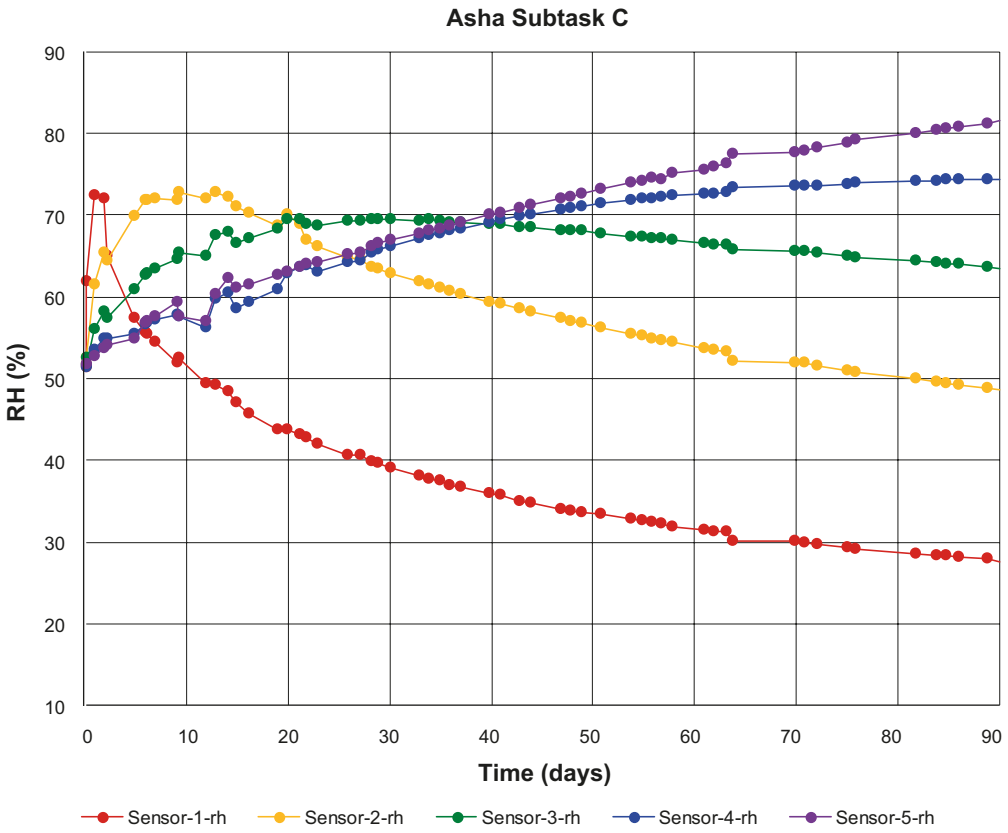

Figure 2-7. *Measured RH vs time in test Ce3d.*

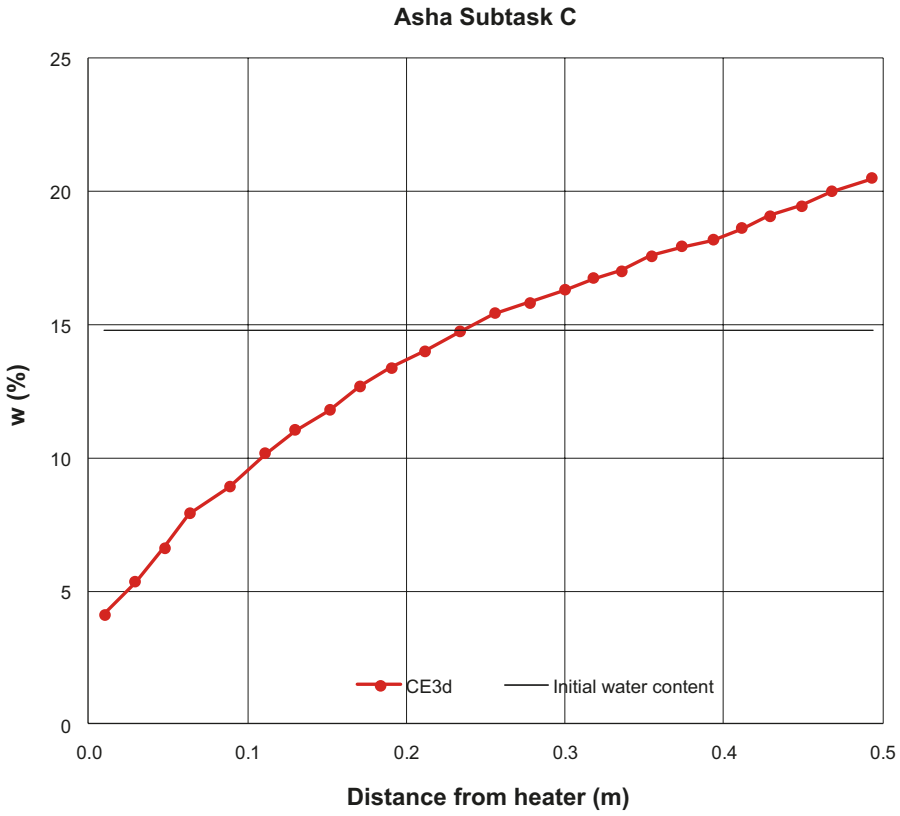

Figure 2-8. *Water content profile at the end of test Ce3d.*

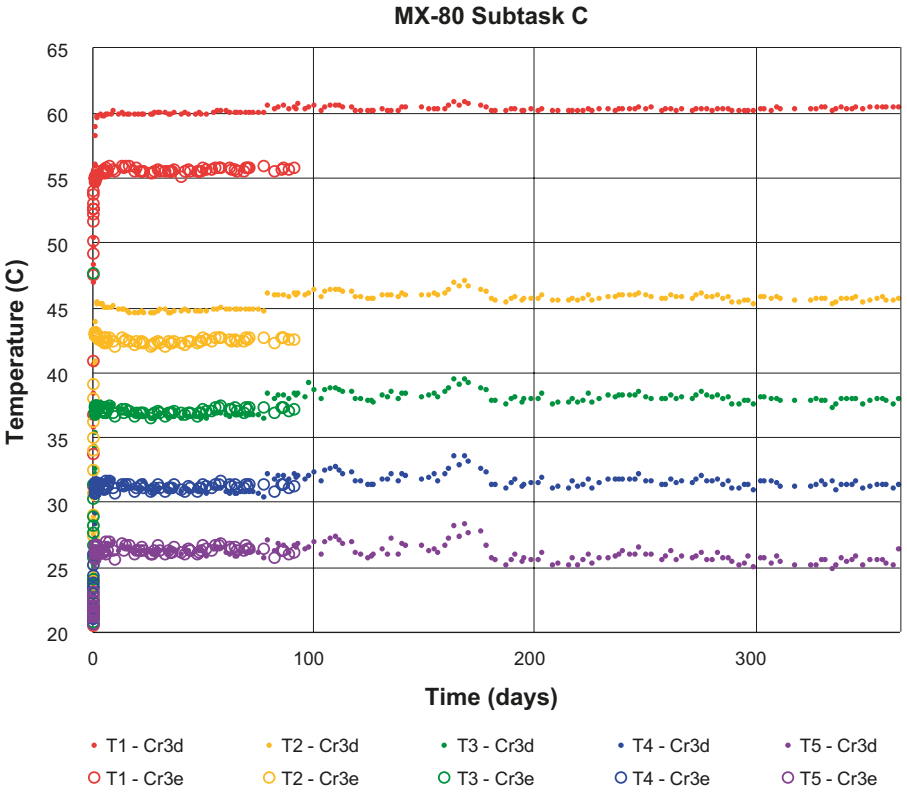

Figure 2-9. *Measured temperature vs time in test Cr3d and Cr3e.*

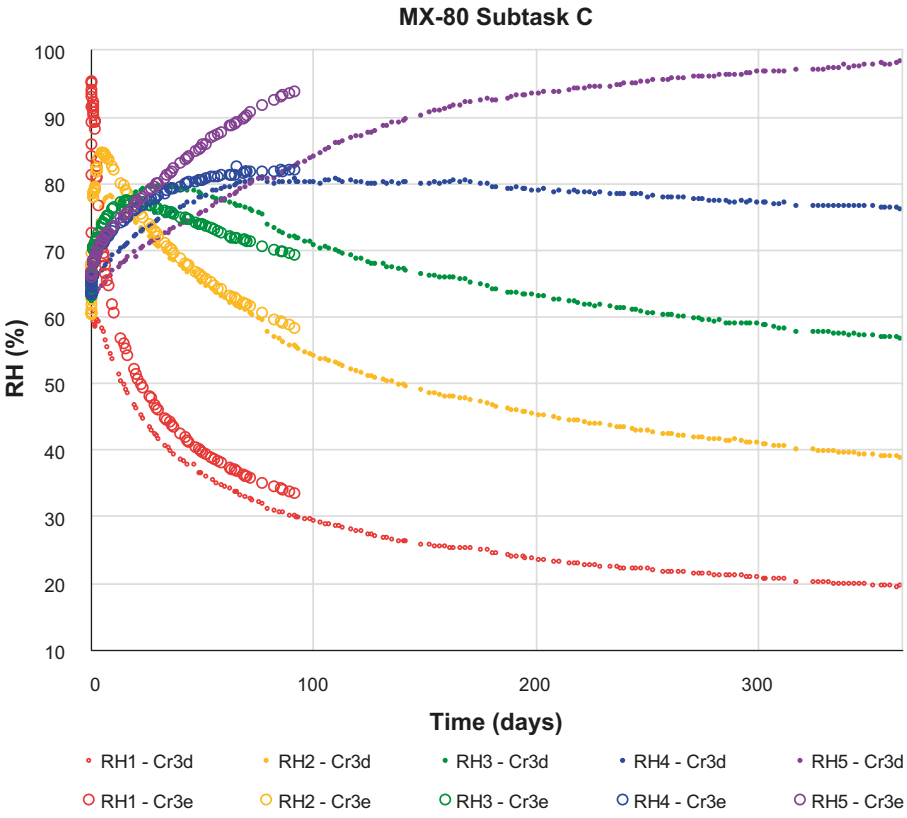

Figure 2-10. *Measured RH vs time in test Cr3d and Cr3e.*

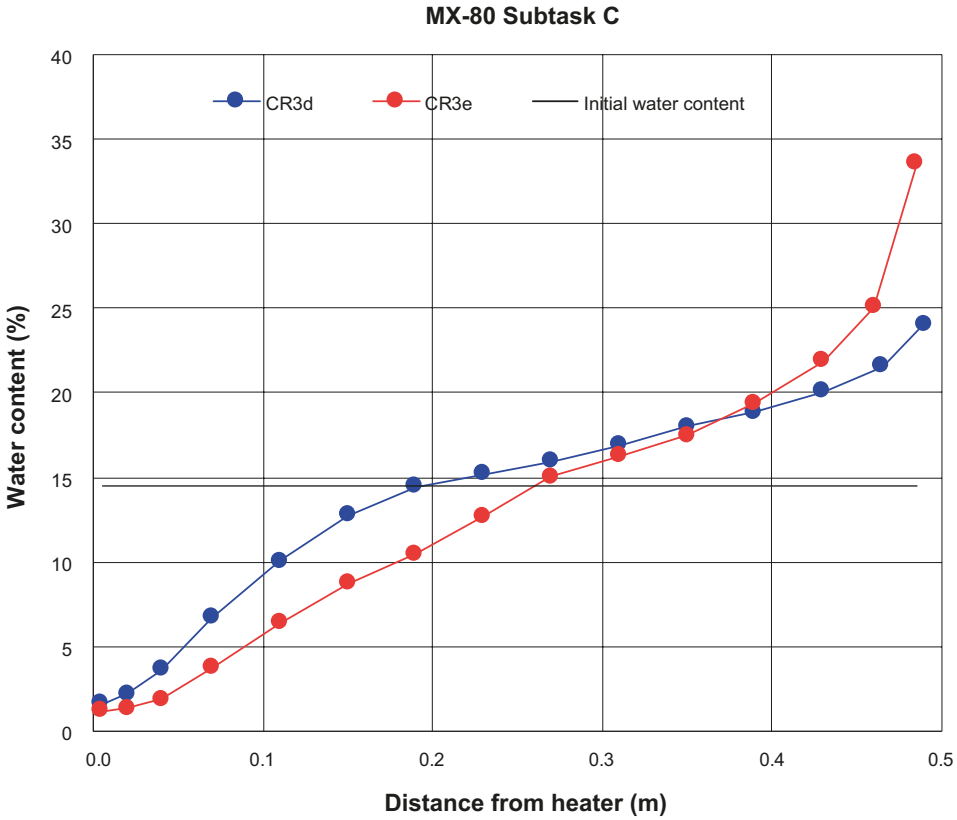

Figure 2-11. *Water content profile at the end of test Cr3d and Cr3e.*

2.4 Requested model results

The scope of the modelling task was focused by requesting results from at least four cases which represented the two subtasks and the two materials. These cases corresponded to the regular long-term water-uptake tests (Ae3 and Ar3), and the thermal gradient tests with the longest duration (Ce3d and Cr3e). The set of experimental data from these tests thereby specified the main part of the requested model results (Table 0-3). Water content profiles from tests with shorter duration (Ae1, Ae2, Ar1, Ar2 and Cr3d) were regarded as representative for the intermediate conditions for three of the model cases.

Table 2-3. Specification of requested results for the different subtasks and materials.

Pellets	Subtask A	Subtask C
Asha	• **Water content vs distance** (0, 5, 30 and 200 days) • **Water uptake vs time** (0–200 days)	• **RH vs time** (0–90 day; 5, 15, 25, 35 and 45 cm) • **Temp vs time** (0–90 days; 5, 15, 25, 35 and 45 cm) • **Water content vs distance** (0 and 90 days)
MX-80	• **Water content vs distance** (0, 5, 30 and 200 days) • **Water uptake vs time** (0–200 days) • **RH vs time** (0–200 day; 3, 8, 15.5 cm)	• **RH vs time** (0–365 days; 5, 15, 25, 35 and 45 cm) • **Temp vs time** (0–365 days; 5, 15, 25, 35 and 45 cm) • **Water content vs distance** (0, 90, 365 days)

3 Model contributions

This chapter presents a short overview of the different modelling contributions and their used codes and materials models, as well as a comparison of these material models.

3.1 SKB

The model contribution from the SKB team was made by using the COMSOL Multiphysics FEM code. Results from four models were submitted corresponding to the four requested cases. Detailed descriptions of the models were presented by Eriksson (2019).

The hydraulic problem was solved by using a complete two-phase flow definition. *The liquid transport* was described with Richard's equation in which the flux is driven by the suction gradient. The flow coefficient included a factor which corresponded to the relative permeability which was defined to be dependent on the contact area between pellets which in turn was calculated from the inter-granule porosity. The hydraulic conductivity was defined as a function of the dry density, which was constant in these models. Finally, the liquid water mass balance equation included a sink/source term which represented the rate of evapouration or alternatively the rate of condensation.

The *gas transport* was described with the Navier-Stoke equation, which is the momentum balance equation, and the Ergun equation, which describes a relation between the pressure gradient, the inter-granule porosity, and the flow velocity. The latter quantity was in turn included in the balance equation for the *water vapour transport*, which included terms for diffusive transport, convective transport and a sink/source term, corresponding to the one in the liquid mass balance. The diffusive transport was driven by gradients in the vapour concentration, and the diffusion coefficient was calculated from the inter-granule porosity.

The *rate of evaporation/condensation* was calculated from the difference between the vapour concentration in the gas phase and the vapour concentration which corresponded to the suction value of the liquid phase.

The *water retention curve* generally described a relation between the water content and the relative humidity (RH). This was defined in such a way that the hysteretic effects from drying and wetting could be taken into account.

The *heat transport* was described with the heat balance equation which included both a convective term and the Fourier´s law. The thermal conductivity was defined to be dependent on the contact area between pellets, which in turn was calculated from the inter-granule porosity.

The *boundary condition* for subtask A was limited to a hydraulic boundary with zero suction. For subtask C the temperatures at the end surfaces were kept constant at 24 and 74 °C, respectively. The lateral sides of the subtask C models were described with a quite low heat transfer coefficient and a defined temperature.

The *geometry* of each model was defined as 2D axisymmetric, and all analyzed models included *gravity*. One model for each modeling case was presented.

3.2 RWM

The model contribution presented by the RWM team from Wood Nuclear Limited was made by using two different codes: the FEM code COMSOL Multiphysics and TOUGH2 code, which uses the integral finite difference method (IFDM). Results from eight models were submitted, corresponding to a set of the four requested cases for each code. Detailed descriptions of the models were presented by Dodd et al. (2019).

In all models, the *liquid transport* was described with Darcy´s law for unsaturated conditions in which the relative permeability was defined as a function of the saturation degree.

Different approaches were however used to describe the *vapour transport*. The COMSOL model of subtask A did not include any representation of vapour transport, whereas the TOUGH2 models for both subtasks included a two-phase flow description, with terms for both diffusive and convective transport. The *gas transport* was described with Darcy´s law and driven by gradients in gas pressure. The diffusive transport was driven by gradients in vapour mass fraction, and the diffusion coefficient was calculated from the porosity and the saturation degree. The vapour concentration was assumed to be in equilibrium with the liquid phase and no term for evaporation/condensation was therefore used. The COMSOL models of the subtask C assumed a constant gas pressure and only included a diffusive term for vapour transport, which was driven by gradients in the fraction between the vapour pressure and the total pressure.

The used *water retention curve* was a so-called extended van Genuchten function which defines the saturation degree as a function of suction.

The *heat transport* was described with the heat balance equation and the Fourier´s law. The thermal conductivity was defined to be dependent on the porosity.

The *boundary condition* for subtask A was limited to a hydraulic boundary with zero suction. The thermal problem for subtask C was simplified by controlling the temperature at the five sensor positions, in addition to the two end surfaces which were kept at 24 and 74 °C, respectively.

The *geometry* of each TOUGH2 model was created as a pseudo 1D computational domain comprised of a vertical stack of 3D grid blocks, whereas actual 1D (line) domains were used for each COMSOL model. All analyzed models included *gravity*. Several additional model cases were also presented: with an alternative (semi constant) water retention curve, with a non-controlled temperature field in subtask C, and cases with the vapour pressure lowering effect (VPL) functionality in TOUGH2 turned off in subtask A.

3.3 SKB 1

The model contribution presented by the SKB1 team from Clay Technology AB was made using the Code_Bright code. Results from five models were submitted: four corresponding to the requested cases and one representing the Cr3d test case. Detailed descriptions of the models were presented by Åkesson (2020).

In all models, the *liquid transport* was described with Darcy´s law for unsaturated conditions in which the relative permeability was defined as a function of the saturation degree. Moreover, all models assumed a *constant gas pressure* and included a *diffusive vapour transport*, driven by gradients in the vapour mass fraction, and described by a diffusion coefficient calculated from the porosity and the saturation degree.

The used *water retention curve* was a so-called extended van Genuchten function which defines the saturation degree as a function of suction.

The *heat transport* was described with the heat balance equation and the Fourier´s law. The thermal conductivity was defined to be dependent on the saturation degree.

The *boundary condition* for subtask A was limited to a hydraulic boundary with zero suction. The initial water uptake in the subtask A tests was considered by adjusting the initial saturation profile for these models. The thermal problem for subtask C was simplified by controlling the temperature at the five sensor positions, in addition to the two end surfaces which were kept at 24 and 74 °C, respectively.

The *geometry* of each model was defined as 1D, and none of the analyzed models included *gravity*. Several additional model cases were also presented: cases without vapour diffusion and without initial saturation in models for subtask A, and cases without internal temperature control in models for subtask C.

3.4 POSIVA

The model contribution presented by the POSIVA team from Universidad de Castilla–La Mancha (UCLM) was made using COMSOL Multiphysics. Results from one model, corresponding to the Ar3 case were submitted. A detailed description of the model was presented by Navarro et al. (2020).

The used constitutive laws were based on a *triple porosity framework* which included one microstructural level and two macrostructural levels, each one represented by a separate set of void ratio, suction and degree of saturation. The microstructural void ratio was defined as water saturated and to be a function of the sum of the suction and the net mean stress (denoted the thermodynamic swelling pressure). A *water retention curve* was defined for each one of the macrostructural levels. The exchange of water between the levels was essentially driven by difference in suction for these levels. The void ratio evolution for each level was governed by the *mechanical processes*, for which the constitutive laws of the BExM was used as a basis.

Liquid transport was defined for the two macrostructural levels and described with Darcy´s law for unsaturated conditions in which the relative permeability was defined as a function of the saturation degree for each level. In contrast, for the microstructural level the water was defined as immobile, albeit exchangeable.

A *constant gas pressure* was assumed, and a *diffusive vapour transport* was defined for each macrostructural level, driven by gradients in the vapour density, and described by a diffusion coefficient calculated from the porosity and the saturation degree, also for each macrostructural level. Taken together, these fluxes are equivalent to the vapour flux for the more conventional description with a single porosity framework (such as the one presented by SKB1).

Gravity was included in the model, and a *hydraulic boundary condition* was applied which corresponded to the water pressure applied at the bottom of the Ar3 test setup.

3.5 Comparison of material models

A compilation of the used constitutive equations is given in Table 3-1. This shows that all presented models included liquid transport driven by suction gradients as described by Darcys´law, and all models included diffusive vapour transport described by Fick´s law except in the COMSOL model of subtask A presented by the RWM team. In contrast, gas transport was only included in two models: in the COMSOL models presented by the SKB team, and in the TOUGH2 models presented by the RWM team. In addition, only the models presented by the SKB team and the POSIVA team included any explicit sink/source terms; in the SKB case for the rate of evaporation/ condensation, whereas in the POSIVA team for the local exchange of water between the different structural levels. These teams also used novel descriptions of the water retention curve. The SKB team used a model in which the water content was defined as a function of the RH, which also incorporated the hysteretic effects. The POSIVA used a model with three structural levels, each one with a relation between suction and the degree of saturation; in the case with the (saturated) micro structure a relation between suction plus the net mean stress and the micro void ratio.

Table 3-1. Constitutive relations used in the differen contributions.

Constitutive equation	SKB1 Code_ Bright	SKB Comsol	RWM Comsol (A/C)	RWM TOUGH2	POSIVA Comsol
Liquid transport (Darcy/Richards)	Yes	Yes	Yes	Yes	Yes
Gas transport	-	Ergun	-	Darcy	-
Vapour transport (Fick´s law)	Yes	Yes	-/Yes	Yes	Yes
Source term	-	Yes	-	-	Yes
Water retention curve	Extended van Genuchten	Hysteresis function	Extended van Genuchten	Extended van Genuchten	Triple porosity model

A similar compilation of additional features of the models is given in Table 3-2. This shows that all presented models included gravity except in the Code_Bright models presented by the SKB1 team. Moreover, the simplification of the thermal problem in subtask C by controlling the temperature at the sensor positions was employed in all models for this subtask, except in the COMSOL model presented by the SKB team. Finally, the approach of adjusting the initial saturation profile in the subtask A models, and thereby taking the initial water uptake into account, was only used in the Code_Bright models presented by the SKB1 team. The triple porosity model presented by the POSIVA team could largely capture this effect due to the preferential flow behavior caused by the structural level associated with the inter-pellets void space.

Table 3-2. Additional features in the differen contributions.

Feature	SKB1 Code_ Bright	SKB Comsol	RWM Comsol	RWM TOUGH2	POSIVA Comsol
Gravity	No	Yes	Yes	Yes	Yes
Controlled temperatures (C)	Yes	No	Yes	Yes	-
Initial water uptake (A)	Yes	No	No	No	No

Compilations of water retention curves and initial conditions, used for MX-80 and Asha pellets respectively, are shown in Figure 3-1. It can be noted that the water retention curves, used by the different teams, in general display similarities. The MX-80 curve used by the RWM team displays slightly lower suction levels, however, and the “high-saturation” part of the curves used by the SKB team display slightly higher suction levels. The effective retention curve resulting from the triple porosity model presented by the POSIVA team displays a slightly higher suction value for saturation degrees in the interval 0.3–0.5 in comparison to the other models. Due to the similarities between the different retention curves and the consistency of the initial water contents in the different models, the initial suction values used by the different groups are also generally quite similar.

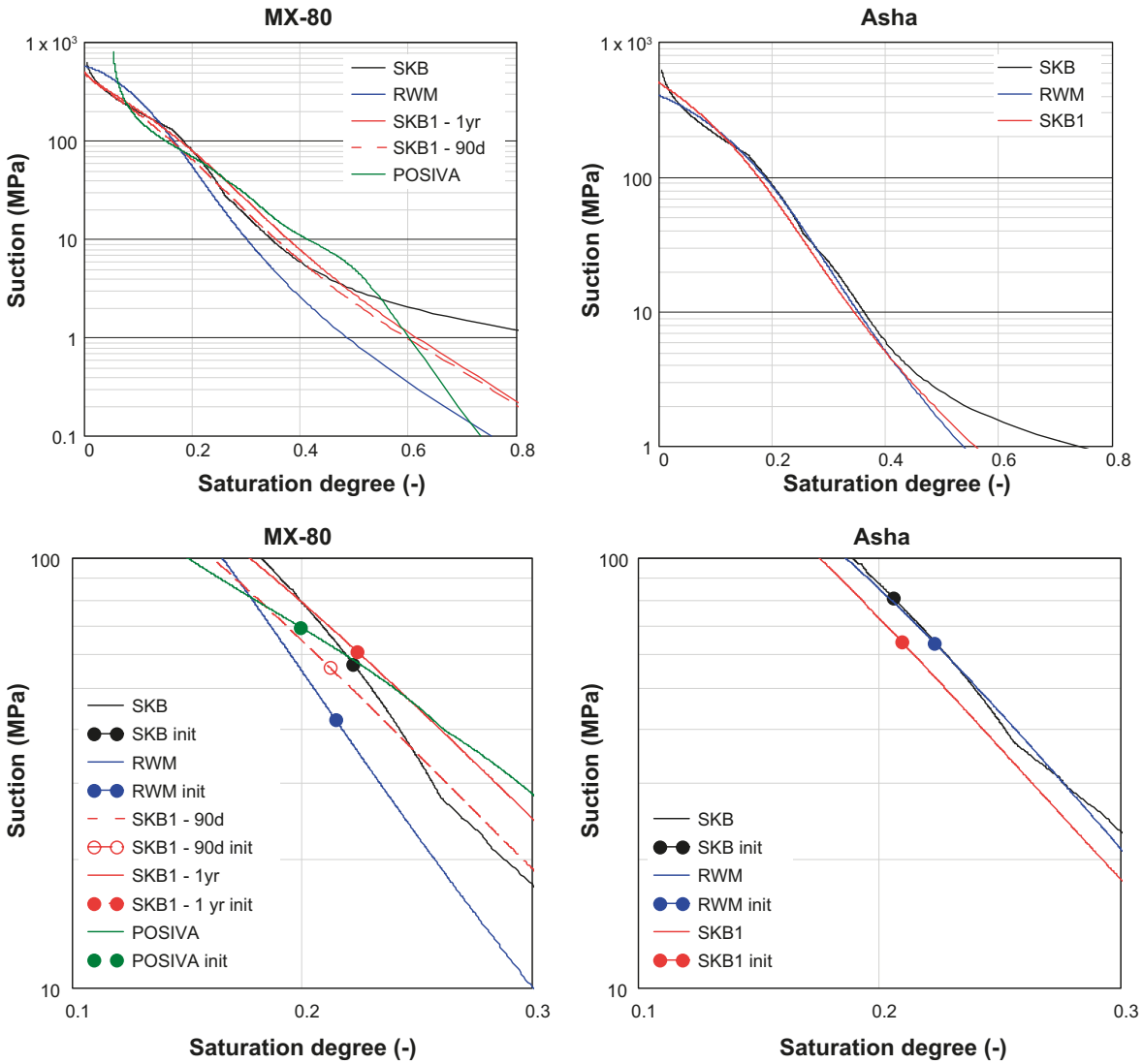

Figure 3-1. *Water retention curves (upper) and initial conditions (middle). Models for MX-80 (left) and Asha (right). The initial conditions were based on reported suction/RH values. The water retention curve for the POSIVA model was based on the assumption that: i) the net mean stress can be neglected, ii) the total void ratio is constant and, iii) that the evolution of the different macrostructural void ratios can be estimated as:* $\Delta e_{M1} = f \cdot \Delta e_M$ *and* $\Delta e_{M2} = -(f + 1) \cdot \Delta e_M$*, where* $f = 0.25$*, which would imply that the* e_{M2} *is essentially depleted for a suction value of 1 kPa.*

Compilations of transport coefficient values are shown in Figure 3-2. The permeability functions used by the different teams shown in the upper row are calculated as the product of the used hydraulic conductivity values and the relative permeability functions. These curves are generally quite similar, with the exception for the MX-80 curve used by the RWM team which displays slightly higher conductivity levels, and especially the curve used by the POSIVA team which displays a threshold for a saturation degree of approximately 0.6 above which the permeability increases strongly with increasing saturation, which was caused by the inter-pellets macrostructural level. This latter approach appears to imply that the overall permeability at saturated conditions may exceed the level expected from experimental hydraulic conductivity values representative for the same overall dry density, even if the microstructural void space will invade the macrostructural void space (especially for the inter-pellets pores M2), and thereby reduce the hydraulic conductivity.

The diffusion coefficients for diffusion of water vapour in air used by the different teams all display a dependence of the temperature (Figure 3-2, lower graph). The illustrated values do not take any influence of the porosity and the saturation degree into account. In general, the values are quite similar, although the values used by the SKB1 and POSIVA teams are approximately 20 % higher than for the other models.

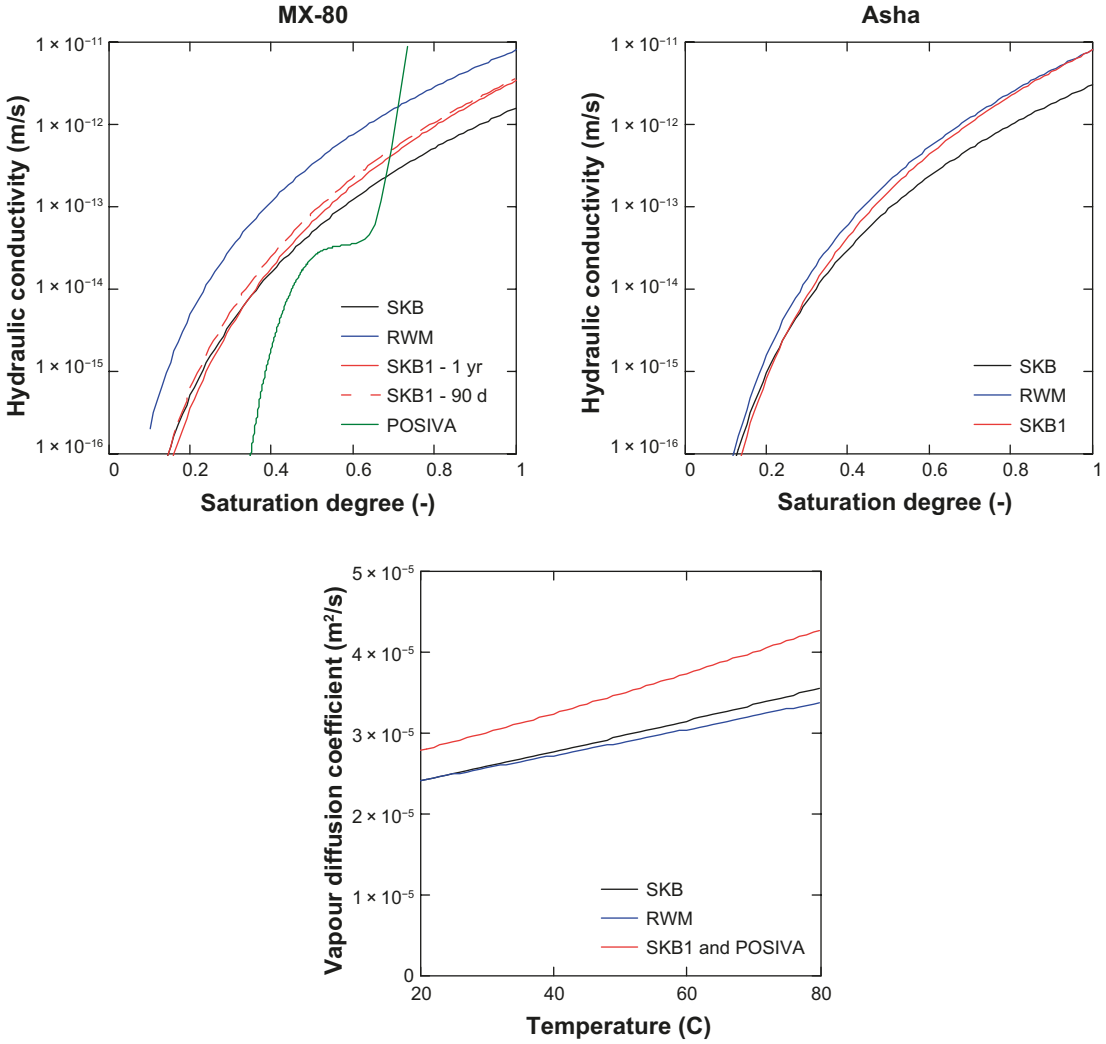

Figure 3-2. *Transport coefficients. Permeability relations, shown as hydraulic conductivity values (upper row) and vapour diffusion coefficients (lower graph).*

4 Results

This chapter presents compilations of model and experimental results for the two subtasks and the two pellets materials, as well as a brief discussion about these results.

4.1 Asha subtask A

A compilation of experimental and modelled water content distributions at different times is shown in Figure 4-1. In general, the model results from the different teams are quite similar, but with a simple comparison by eye the model by the SKB team appears to coincide with the experimental data most closely, especially regarding the results for 5 and 200 days. The models by the RWM team are also very close for all three dates. The initial water content profile in model by the SKB1 team reflects the approach with an initial water uptake and is therefore quite different than the other models. The modelled water contents for day 5 and day 30 are significantly higher than the measured data, but since these results were obtained from tests with lower boundary pressure and less initial water uptake, it is not really relevant to compare this model with the experimental data for day 5 and 30.

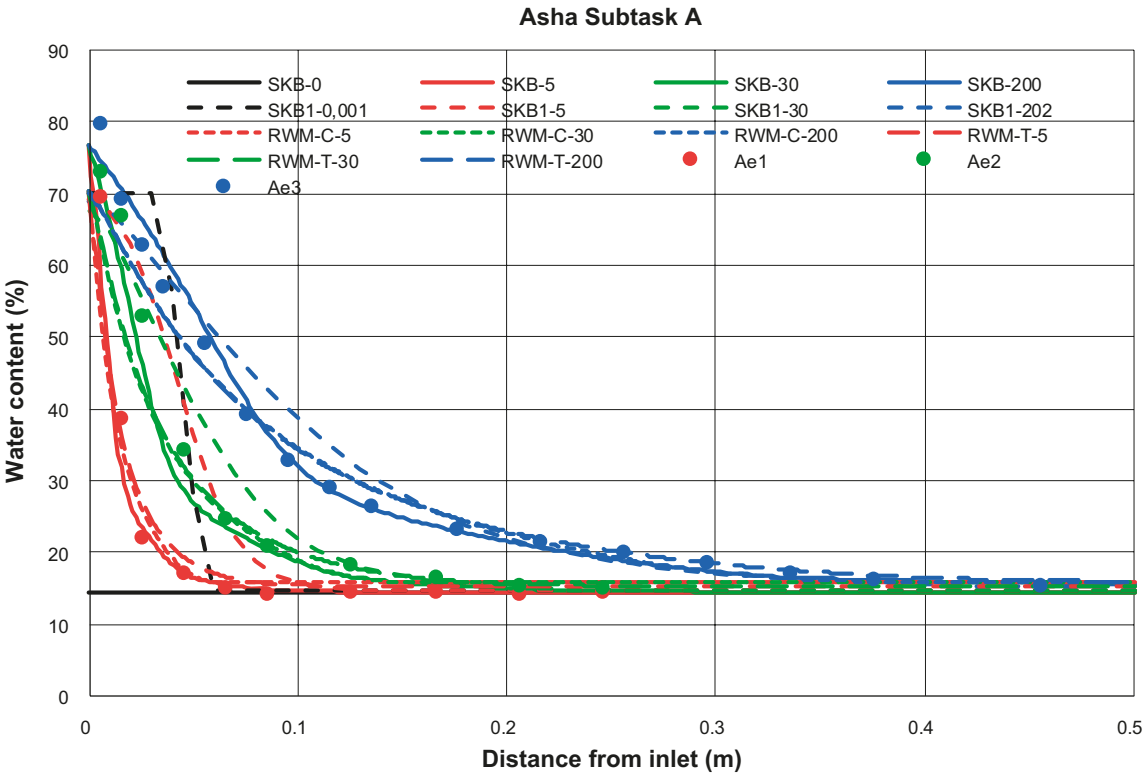

Figure 4-1. *Water content distributions for Test type A with extruded pellets with Asha.*

Modelled and measured evolutions of the cumulative water uptake are shown Figure 4-2. The initial water uptake considered in the model by the SKB1 teams means the result from this model is quite similar to the first measured values of the uptake. However, at the end of the test the experimental and the model results have deviated with approximately 150 g, and this difference is thought to be caused by different types of evaporation and leakage. The model presented by the SKB team started from a zero uptake. Initially, however, it displayed a water uptake rate significantly higher than the SKB1 model which meant that the cumulative uptake for these two models with time displayed quite similar trends. The results presented by the RWM teams was very similar to SKB model but was simply shifted upwards to coincide with the initial measured uptake data.

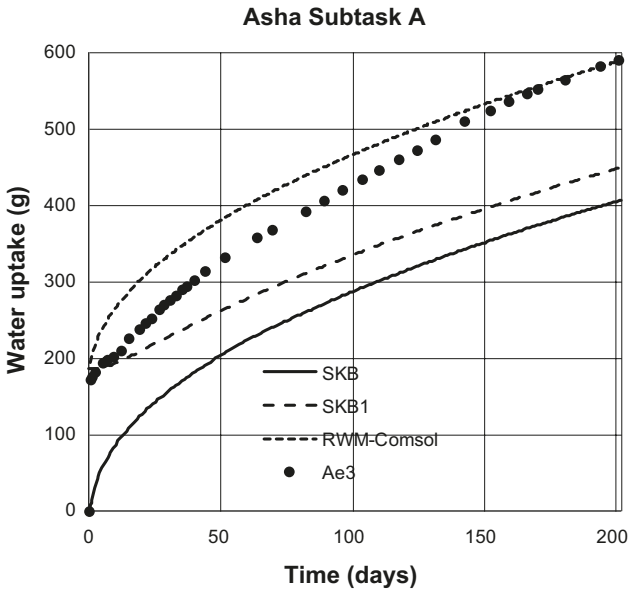

Figure 4-2. *Water uptake for Test type A with extruded pellets with Asha.*

4.2 MX-80 subtask A

Compilation of experimental and modelled results for the water contents distribution and the cumulative uptake at different times is shown in Figure 4-3, Figure 4-4 and Figure 4-5, respectively. In general, these models and test results displayed comparable similarities and differences as for the tests performed with Asha bentonite. The model presented by the POSIVA team displayed a rapid and fairly accurate cumulative water uptake, and this is also to some extent reflected in the salient water content profile after 5 days. However, the rapid uptake continued, which meant that the final water content distribution after 200 days was quite high in comparison with the measured water content profile for that time.

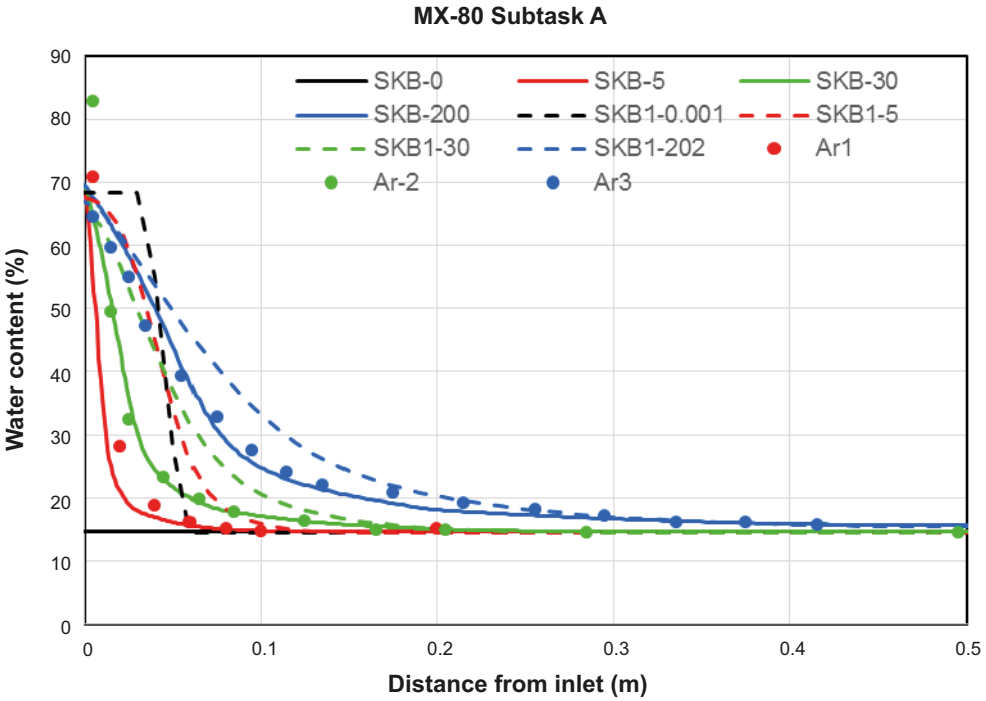

Figure 4-3. *Water content distributions for Test type A with roller compacted pellets with MX-80.*

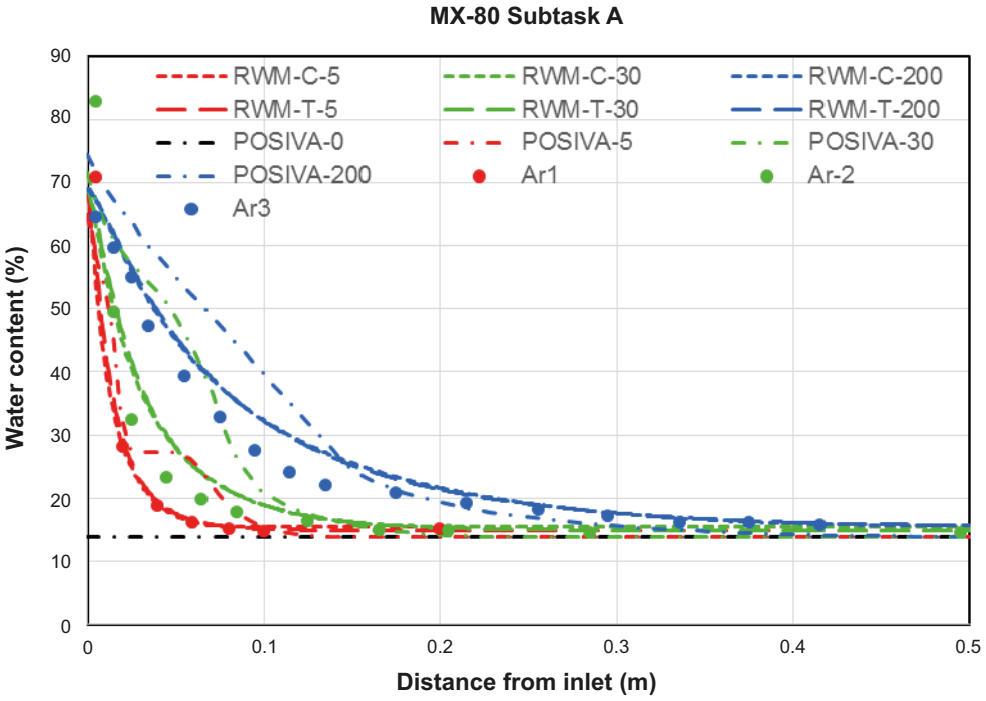

Figure 4-4. *Water content distributions for Test type A with roller compacted pellets with MX-80 (continuation).*

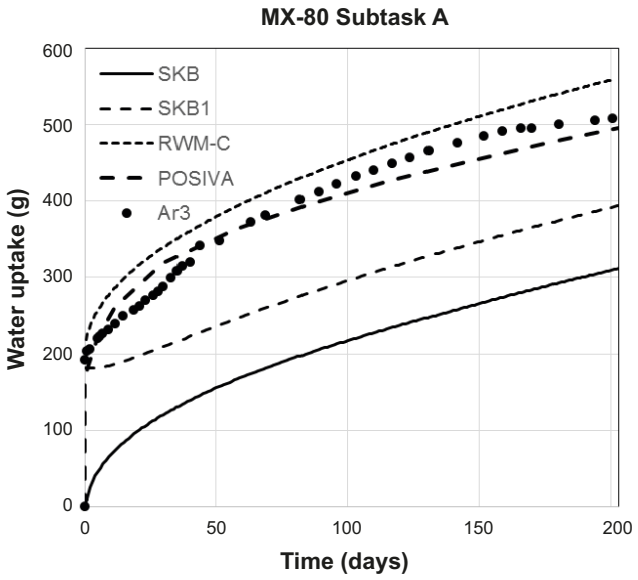

Figure 4-5. *Water uptake for Test type A with roller compacted pellets with MX-80.*

Modelled and measured evolutions of the relative humidity at the three sensor positions are shown in Figure 4-6 and Figure 4-7. The experimental data for sensor 3 cm from the inlet shows that this was flooded immediately. This supports the approach with the initial water uptake, which was pursued by the SKB1 teams. The model results presented by the SKB team also displayed a very fast increase to saturated conditions. For 8 cm from the inlet, all presented models displayed RH evolutions which were quite similar to the experimental data. The model presented by the SKB team captured however the sensors data most closely. For 15.5 cm from the inlet, the presented model by the SKB1 team followed the sensors data most closely. This supported the approach with an initial water uptake and the notion that the vapour diffusion had a significant influence on the moisture transport. The model presented by the POSIVA team displayed a fairly accurate RH evolution at 3 and 8 cm from the inlet, but tended to underestimate the RH evolution at 15.5 cm from the inlet. This and the over-estimated water contents at 200 days is consistent with a retention curve which appears to overestimate the suction level for saturation degrees in the interval 0.3–0.5 (Figure 3-1). The initial RH level in the models presented by the RWM team was slightly higher than the sensor data, and this corresponds to the relativley low initial suction value shown in Figure 3-1.

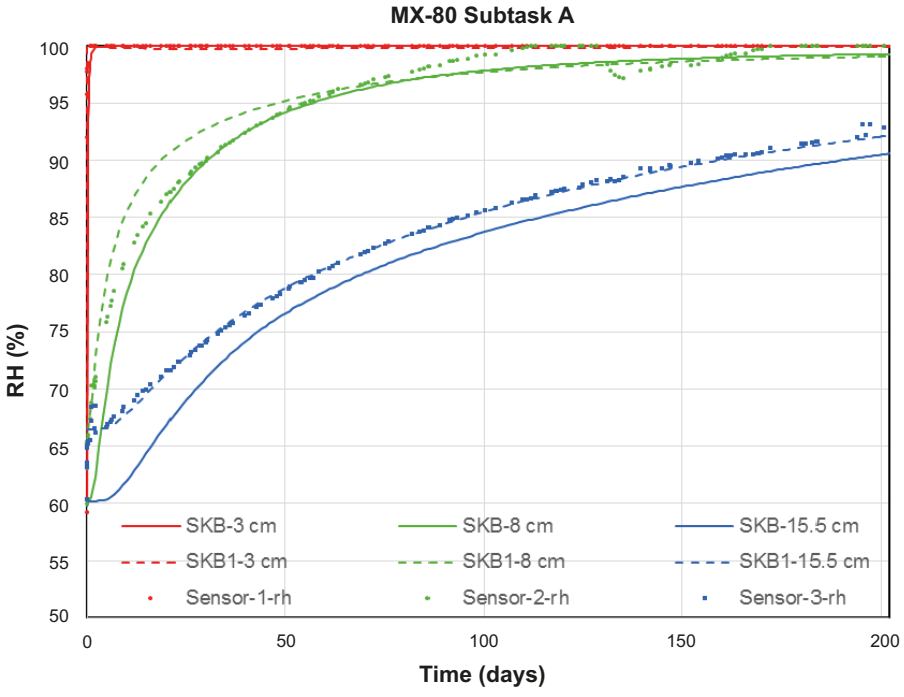

Figure 4-6. *RH evolution for Test type A with roller compacted pellets with MX-80.*

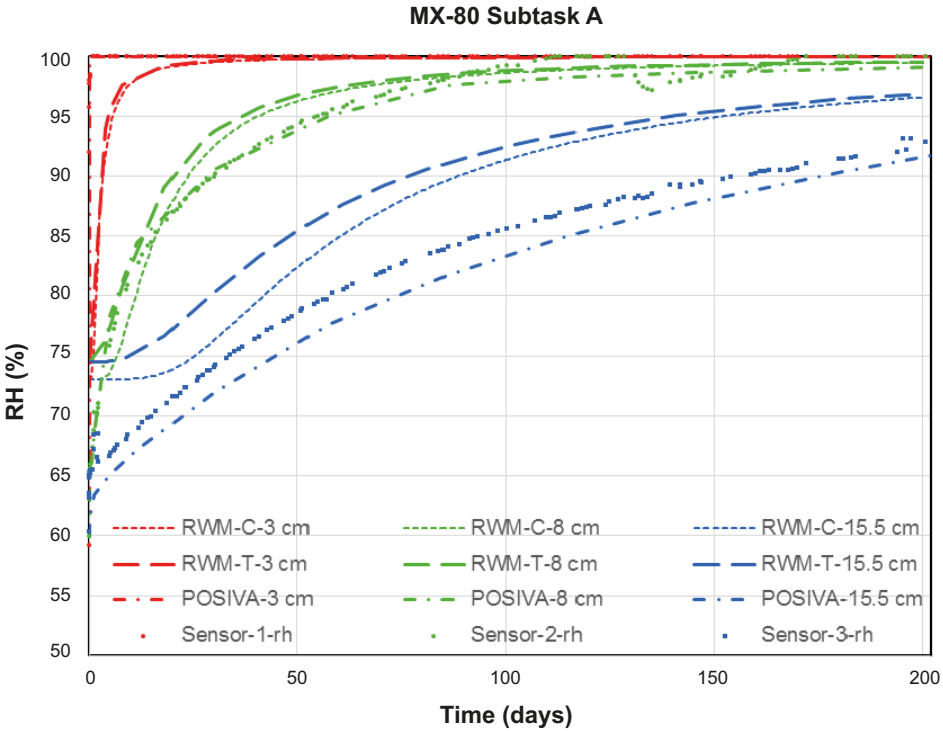

Figure 4-7. *RH evolution for Test type A with roller compacted pellets with MX-80 (continuation).*

4.3 Asha subtask C

Modelled and measured evolutions of the relative humidity at the five sensor positions are shown in Figure 4-8. In general, the different models display many similarities regarding the time scale and the final distributions, although some deviations can be noted. The models presented by the RWM team captured the sensors data most closely, especially at 15, 25 and 35 cm from the heater. In contrast, the model presented by the SKB team displayed significantly lower RH values at 5 and 15 cm from the heater. These low RH levels were possibly caused by the fact that the water retention curve was defined for RH rather than for suction, and that the temperature effect implied by the Kelvin´s equation does not come into play.

Modelled and measured evolutions of the temperature at the five sensor positions are shown in Figure 4-9. The results from the models presented by the RWM team and the SKB1 team are, as expected, very close to the experimental data which was due to the control of the thermal conditions in these models. The model results presented by the SKB team were generally within 3 °C from the experimental data.

Modelled and measured distributions of the water content at the end of the tests are shown in Figure 4-10. In general, the models displayed quite similar results and good agreement with experimental data. A minor general overestimation is however consistent with a loss of water of approximately 4 % estimated from the experimental data (Åkesson et al. 2020).

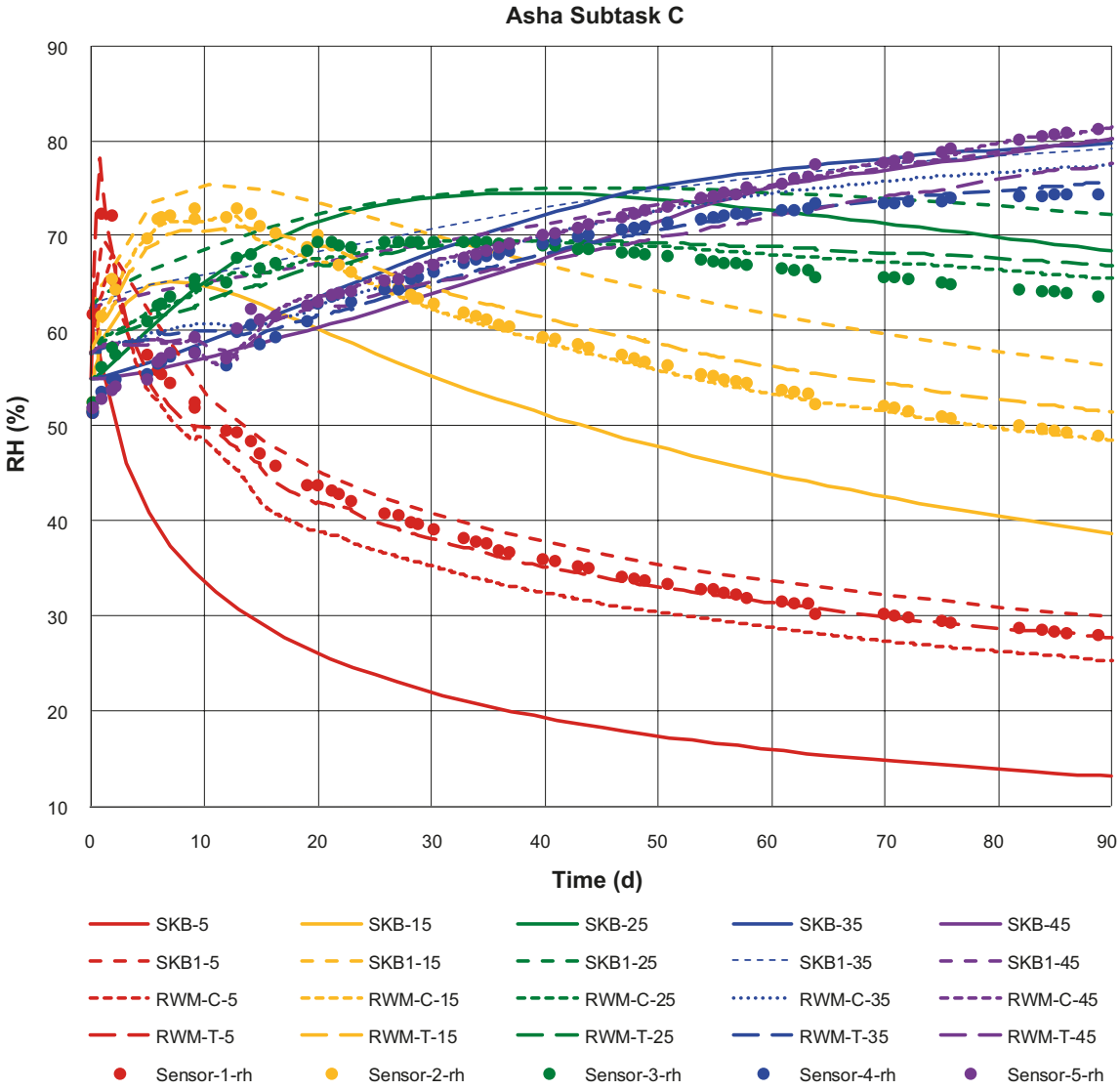

Figure 4-8. *RH evolution for Test type C with extruded pellets with Asha.*

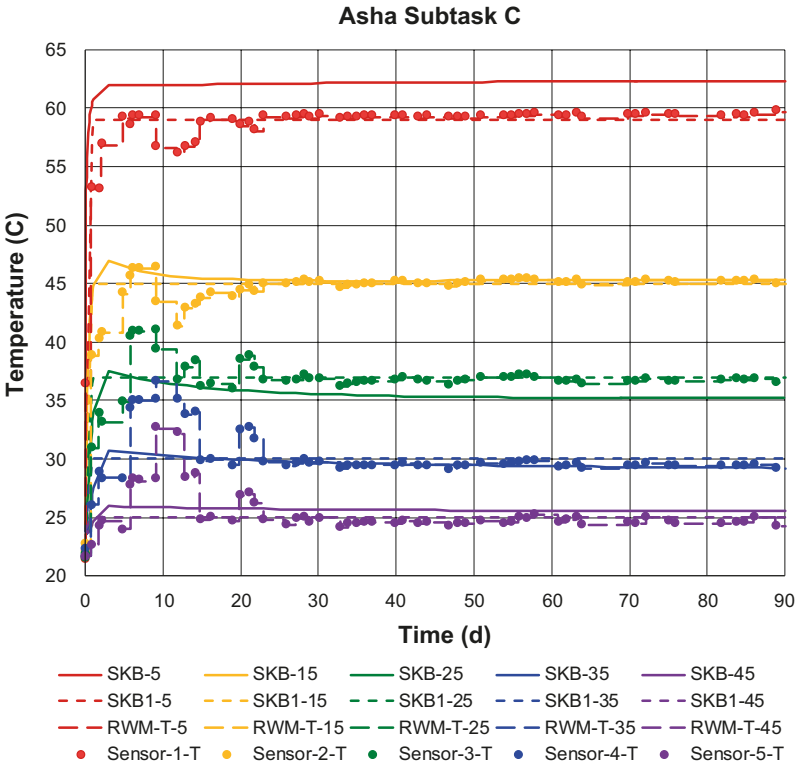

Figure 4-9. *Temperture evolution for Test type C with extruded pellets with Asha.*

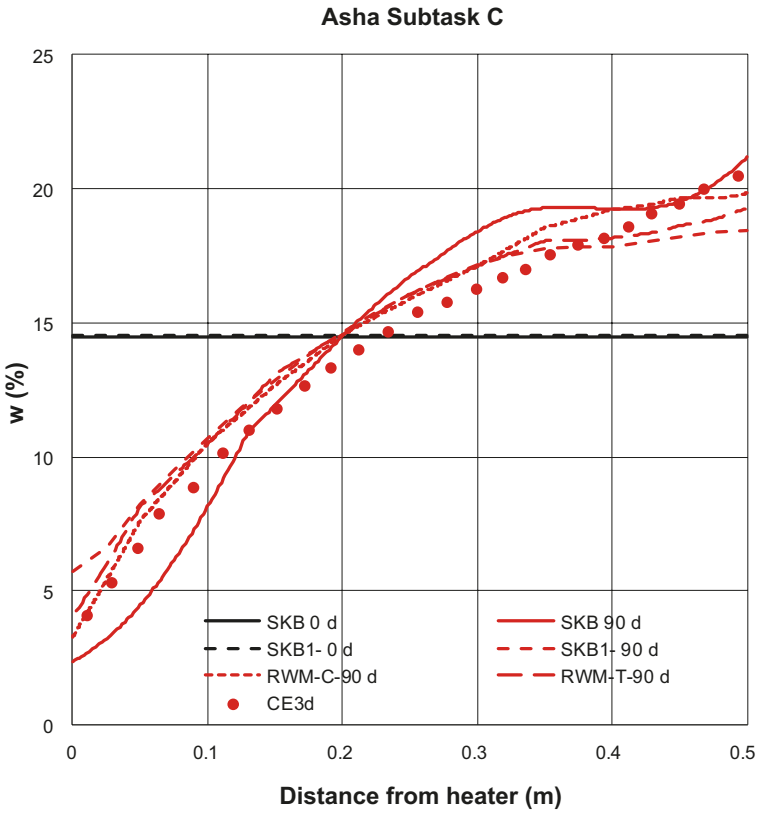

Figure 4-10. *Water content distributions for Test type C with extruded pellets with Asha.*

4.4 MX-80 subtask C

Modelled and measured evolutions of the relative humidity at the five sensor positions are shown Figure 4-11. In general, as with the results for the test with Asha material, the different models display many similarities regarding the time scale and the final distributions. The model presented by the SKB team displayed significantly lower RH values at 5, 15 and to some extent 25 cm from the heater. Moreover, the rate of change displayed by this model at the end of the test, especially at 25 and 35 cm from the heater, was significantly higher than for the experimental data and for the other models.

Modelled and measured evolutions of the temperature at the five sensor positions are shown in Figure 4-12. The results from the models presented by the RWM team and the SKB1 team are, as for the test with Asha material, very close to the experimental data. The model results presented by the SKB team were generally within 3 °C from the experimental data.

Modelled and measured distributions of the water content at the end of the tests are shown in Figure 4-13. Experimental data from the two tests Cr3d and Cr3e are shown. These two data sets correspond to model results for two different times 90 and 365 days (indicated with blue and red, respectively), which both are presented for the models from the SKB and SKB1 teams, while only the latter time is presented for the models from the RWM team. For the data sets representing results after 90 days, a quite good agreement can be noted for both (SKB and SKB1) models. After 365 days, however, the model results deviated to some extent from each other and from the experimental data. Especially at the cold end, quite significant differences were observed for the model presented by the SKB team.

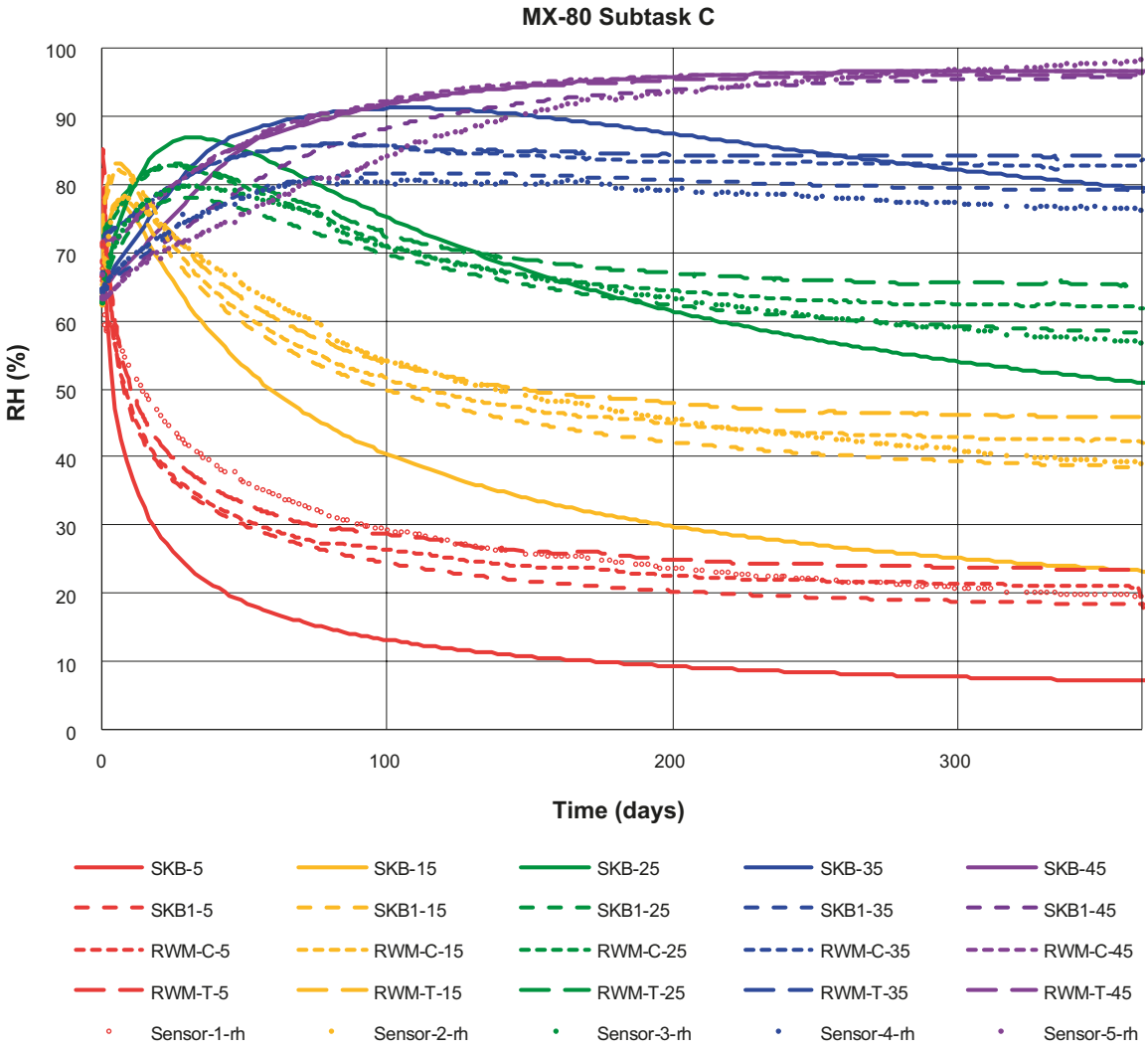

Figure 4-11. *RH evolution for Test type C with roller compacted pellets with MX-80.*

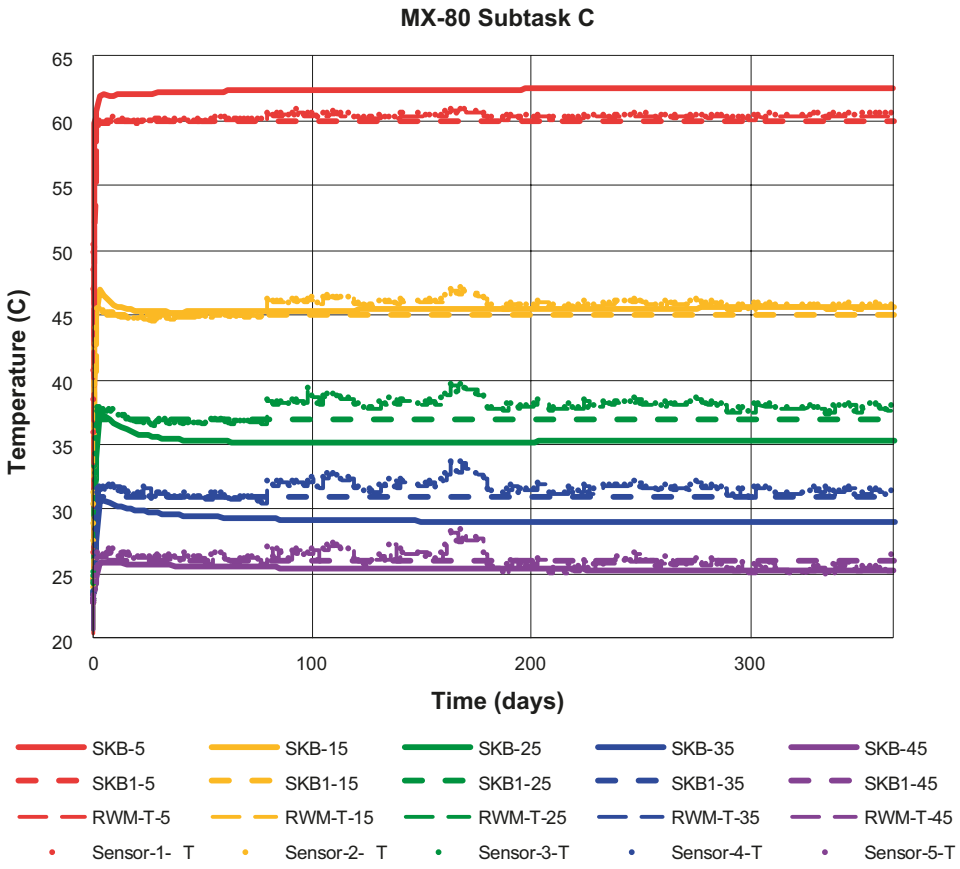

Figure 4-12. *Temperature evolution for Test type C with roller compacted pellets with MX-80.*

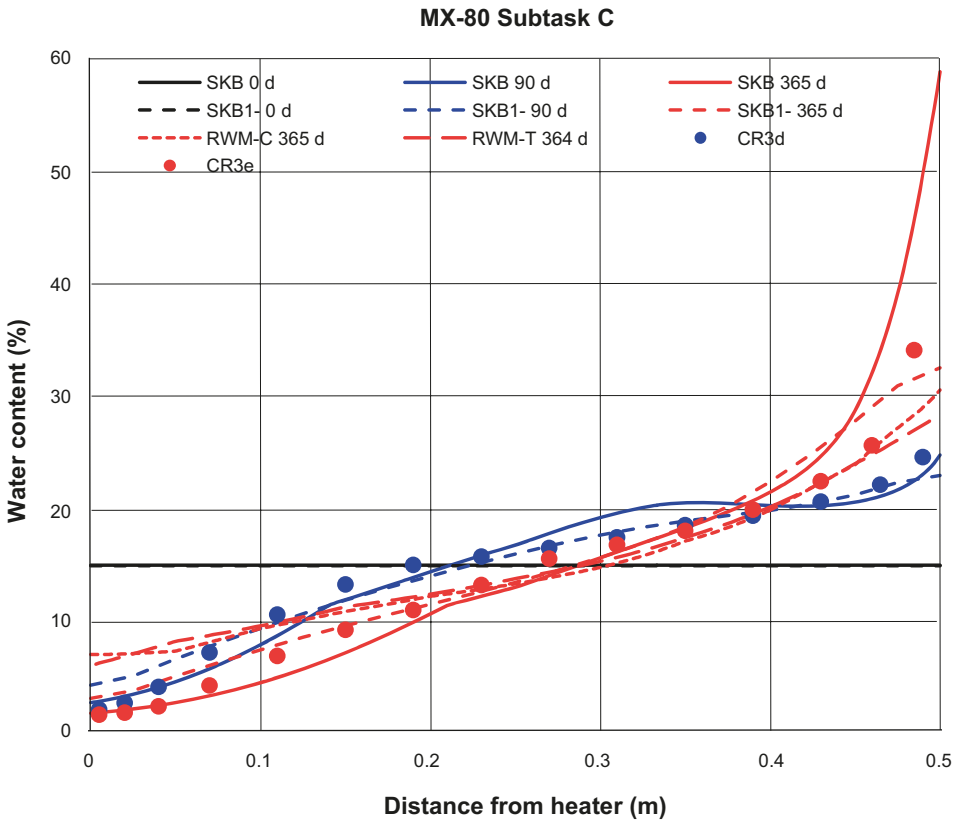

Figure 4-13. *Water content distributions for Test type C with roller compacted pellets with MX-80.*

4.5 Discussion

The results presented by the different modelling teams have generally exhibited many similarities, even though different modelling approaches have been used. The following approaches were found to have a negligible influence on the results in both subtasks: i) the inclusion of gas transport, which means that it is safe to assume a constant gas pressure; ii) the inclusion of a source term for evaporation/condensation, which means that equilibirium between the water in the macro pores and the interlayers can be assumed; and iii) the inclusion of gravity, which means that this can be safely disregarded.

Other approaches were found to have a significant influence on the model results: i) The initial water uptake in subtask A was considered by the SKB1 team. This approach appeared to be necessary in order to replicate the RH evolution, especially at 15.5 cm distance for the inlet; a similar behavior was displayed by model from the POSIVA team, which incorporated a preferential flow behavior caused by the structural level associated with the inter-pellets void space. ii) A controlled temperature field in subtask C meant that the uncertainties related to the thermal problem in the bentonite and the insulation could be avoided. Åkesson (2020) found that this approach had an influence on the hydraulic evolution, although not necessarily that the hydraulic results were improved by it; iii) The used water retention curve used by the SKB team appears to have led to an exaggerated divergence of the RH levels in subtask C. This was possibly an effect of defining the water retention curve as a function of RH rather than of suction; iv) One of the models (SKB) displayed an extensive water accumulation after one year at the cold end in subtask C with MX-80 (Cr3e). This behavior could possibly be a consequence of the used water retention curve, and the high suction level at high saturation degrees displayed by this curve (see Figure 3-1).

Finally, the contribution of vapour diffusion on the overall moisture transport in subtask A was investigated by Åkesson (2020), and it was found that vapour diffusion has a significant influence at low water content. The analysis presented by Dodd et al. (2019) indicated, on the other hand, that the vapour diffusion had a quite insignificant influence on the moisture transfer in the subtask A tests.

5 Concluding remarks

The presented modelling work has shown that the established TH models can essentially describe the processes in both the investigated test types.

Test conditions defined by the pressure boundary (subtask A) or the temperature profile (subtask C) mean that the processes are slow enough to sustain a thermodynamic equilibrium between water activity in macro pores and in the interlayer clay water (Figure 5-1 upper panels). Macro-pores are therefore essentially gas-filled which means that the water transport is governed by the same interlayer HM mechanisms which determine the hydraulic conductivity at saturated conditions.

Established TH models are not sufficiently suited for conditions in which the inflow rate is governed by an external process, i.e. test type B. A typical example of such a situation is the localized water inflow into a pellets-filled slot through a fracture intersecting a deposition hole. This will imply the non-equilibrium between macro pores and the interlayer, which in turn can lead to water transport through the macro-pores (Figure 5-1 lower panel).

The model presented by the POSIVA team was based on a different description in which liquid water transport occurred both inside the pellets (without the contribution of the microstructural water), and between the pellets. The main difference in comparison to the conditions outlined in Figure 5-1 (lower panel), was that the inter-pellets liquid transport could play a prominent role even though the water in the different structural levels were in equilibrium.

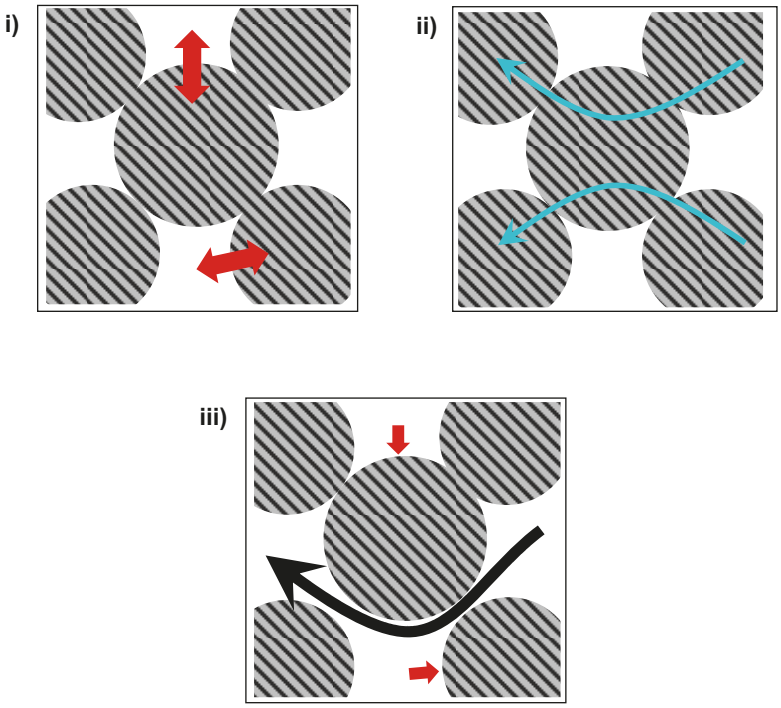

Figure 5-1. *Schematic illustration of water-filled micro-pores in pellets and macro-pores. Condition with equilibrium between pore systems (i), water transport through micro-pores (ii), and condition without equilibrium and with water transport through macro-pores (iii).*

The presented models have shown that vapour transport governed by diffusion is a quite accurate and sufficient description of the processes in the investigated test types. However, this result may be due to the situation in which the temperature gradient is parallel to the direction of gravity. If these vectors would be perpendicular, which is largely the case in the pellets-filled slot in a deposition hole, then it can be expected that influence of natural convection would be more significant (Figure 5-2).

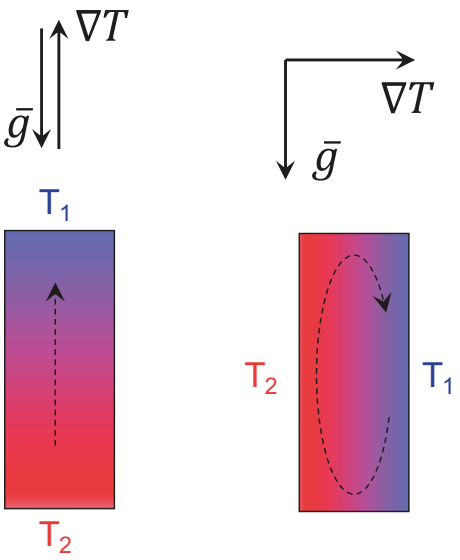

Figure 5-2. *Schematic illustration of expected influence of gravity on vapour transport, parallel and perpendicular to thermal gradient.*

References

SKB's (Svensk Kärnbränslehantering AB) publications can be found at www.skb.com/publications.

Dodd J, Tsitsopoulos V, Hoch A, Holton D, Åkesson M, 2019. Modelling water transport in bentonite pellets: Task 10 of the EBS Task Force. Wood report 204127-AA-UA00-00001-06-1, Wood, UK**.**

Eriksson P, 2019. Development of thermo-hydraulic model for pellet fillings. SKB P-19-12, Svensk Kärnbränslehantering AB.

Navarro V, Asensio L, Gharbieh H, De la Morena G, Pulkkanen V-M, 2020. A triple porosity hydro-mechanical model for MX-80 bentonite pellet mixtures. Engineering Geology 265, 105311. doi:10.1016/j.enggeo.2019.105311

Åkesson M, 2020. EBS TF – THM modelling. Water transport in pellets-filled slots. Modelling of test cases A and C. SKB P-20-19, Svensk Kärnbränslehantering AB.

Åkesson M, Goudarzi R, Börgesson L, 2020. EBS TF – THM modelling. Water transport in pellets-filled slots. Laboratory tests and task description. SKB P-19-06, Svensk Kärnbränslehantering AB.

Arkitektkopia AB, Bromma, 2020

SKB is responsible for managing spent nuclear fuel and radioactive waste produced by the Swedish nuclear power plants such that man and the environment are protected in the near and distant future.

skb.se